Heliyon 5 (2019) e02903

Contents lists available at ScienceDirect

Heliyon

journal homepage: www.cell.com/heliyon

Research article

A DFT study on functionalization of acrolein on Ni-doped $(ZnO)_6$ nanocluster in dye-sensitized solar cells

S. Dheivamalar [a,*], K. Bansura Banu [b]

[a] PG and Research Department of Physics, Periyar E.V.R. College (Autonomous), Tiruchirappalli, 620023, India
[b] PG and Research Department of Physics, Holy Cross College (Autonomous), Tiruchirappalli, 620002, India

ARTICLE INFO

Keywords:
Materials chemistry
Nanotechnology
Optics
Theoretical chemistry
DSSC
NiZn5O6
DFT
Adsorption
Density of states

ABSTRACT

In this work, the functionalization of Acrolein on the Nickel-doped Zn_6O_6 (A-$NiZn_5O_6$) nanocluster with different adsorption configurations (C, M_1 & M_2) as the π conjugated bridging in dye-sensitized solar cells (DSSC) compared with the anchoring group [6,6] - phenyl-C_{61}-butyric acid methyl ester (PCBM) have been investigated through (DFT/TD-DFT)) calculations by Gaussian 09 program. The interaction between the $NiZn_5O_6$ and the Acrolein has been explored through three functional groups are = O Carbonyl group (C), –CH Methyl group (M_1), and –CH_2 Methylene group (M_2) of the Acrolein. The nature of the interaction between the Acrolein and $NiZn_5O_6$ has been exhaustively studied in terms of energy gap (E_g), global reactivity descriptors, molecular geometries, adsorption energy, the density of states, Mulliken atomic charges, molecular electrostatic potential, and the UV-Vis spectra for each adsorption site. The frontier molecular orbital analysis study indicated that all dyes could give a suitable electron vaccination from the LUMO orbital of A-$NiZn_5O_6$ to the HOMO orbital of PCBM. The adsorption process significantly improved the incident photon to the current conversion potency of the A-$NiZn_5O_6$. The determination of density functional theory calculations revealed that the C site of A-$NiZn_5O_6$ material was faced with a lower chemical hardness and energy gap (E_g) as well as a higher electron accepting power and light harvesting efficiency compared to other sites.

1. Introduction

Dye-sensitized solar cells are the real substitutes to the well-established silicon-hinge solar cells owing to their greater occurrence of the photon to current transformation potency, low cost, ease of gadget invention and long-term stability [1]. The implementation of DSSC is primarily focused on the integration of photons throughout the complete visible and near-infrared regions, dye-sensitizers attached to the upper-most layer of anchoring group, the unoccupied energy level above the occupied level of PCBM and the electrolyte containing redox system [2]. The π-conjugated elements are used to stimulate the photosynthetic process on account of their superior electrochemical properties. The sensitizer interacts with the semiconductor through the PCBM, which enhances the light harvesting ability, the electron injection, the stability and the production of solar cells. Researchers are majorly concentrated on progressing dyes of structural unit donor - π - acceptor configurations [3].

The ZnO nanoparticles have attained the major attention of researchers due to their potential applications in the field of electronics, material science, and medicine [4]. The Zinc Oxide nanoparticles are highly attractive materials because it finds remarkable uses in piezoelectric devices, UV absorbers, sensors, pharmaceuticals, and cosmetic industries [5]. These nanostructured materials are of greater importance owing to their nano morphology, nontoxicity, functionality, and biocompatibility [6]. The ZnO nanostructured material has an immense band gap of 3.3 eV, which makes this material as the best semiconductor with the highest acceptance binding energy of 60 MeV in addition to low lasting threshold [7, 8]. Nano-scale Ni is a latent positive p-type semiconductor material, and its properties are one of the most important factors to influence the performance of photovoltaic devices. Doping such metal cation is an effective way to improve the electrochemical performance. This improved activity has been attributed to the enhanced separation of photogenerated electron-hole pairs due to the presence of Ni^{2+} ions in ZnO [9]. The change of semiconducting behavior of ZnO has been attributed to the Ni dopant. It has been reported that Nickel doped ZnO with a smaller crystalline size shows better electrical, optical and

* Corresponding author.
E-mail address: sitrulinsiragugal@gmail.com (S. Dheivamalar).

https://doi.org/10.1016/j.heliyon.2019.e02903
Received 2 February 2019; Received in revised form 3 June 2019; Accepted 18 November 2019

magnetic properties [10]. To further enhance the electrochemical performance of Ni- doped Zn_6O_6, Acrolein molecule is adsorbed on the surface of nano-scale $NiZn_5O_6$. Acrolein comprises of adjacent C=C and C=O double bonds in conjugation. The deals-alder reaction of Acrolein enhances the property of interacting with $NiZn_5O_6$ [11, 12]. Mehdi *et.al* had analyzed the DFT calculations to investigate the Acrolein interaction with COOH loaded single-walled CNT [13].

A noteworthy attentiveness is on A-$NiZn_5O_6$ as photosensitizing dyes that are strongly absorbed the photons. The A-$NiZn_5O_6$ composite leads to a photoactive compound capable of electron transfer due to photoexcitation. During this investigation, the electronic structures, photovoltaic properties of A-$NiZn_5O_6$ were studied at various interaction sites to determine their potential effectiveness in dye-sensitized solar cells by the DFT/TD-DFT calculations. The effects of Ni doping and Acrolein adsorption on the nano-scale Zn_6O_6 have not to be reported yet. We surmise that this work will provide some basic guidelines to experimentalists to strengthen the implementation of DSSCs.

2. Theoretical methods

The geometrical framework of $NiZn_5O_6$ and A-$NiZn_5O_6$ were optimized using the B3LYP/6-31G exchange-correlation functional method with 6-31G (d,p) basis set using the Gaussian 09 program [14]. The TD-DFT computations were employed to evaluate the excitation energy, UV-Vis electronic transition, light harvesting ability and oscillator strength of photosensitizer at CAM-B3LYP/6-31G level. The HOMO/-LUMO energies were analyzed at the B3LYP/6-31G level with optimized structures. The Gauss sum program was used to obtain DOS results [15]. The dipole moment, chemical parameters and polarizability were predicted from the B3LYP/6-31G functional in Gaussian 09 program. In further, molecular electrostatic potential (MEP) analysis and Mulliken charge distribution of each atom in the various sites of A-$NiZn_5O_6$ were also investigated by the Gaussian 09 program. The adsorption energy (E_{ad}) of Acrolein on the $NiZn_5O_6$ at different configurations is represented by,

$$E_{ad} = E_{A\text{-}NiZn5O6} - (E_{NiZn5O6} + E_A) \quad (1)$$

Where,

$E_{A\text{-}NiZn5O6}$ is the total electronic energy of the Acrolein adsorbed over the $NiZn_5O_6$ nanocluster,
$E_{NiZn5O6}$ is the total energy of the $NiZn_5O_6$ nanocluster,
E_A is the total energy of the isolated Acrolein molecule [16].

3. Results and discussion

3.1. Structural properties

The complex A-$NiZn_5O_6$ is capable of absorbing the photons of light. Computational methods (TD-DFT/DFT) were used for characterizing A-$NiZn_5O_6$ with various interaction sites. The geometrical profile of $NiZn_5O_6$ is seen in Figure 1. The 3D structure of Zn_6O_6 was composed of two tetragonal rings faced one another that is coupled by Zn–O bonds. The Zn–O bond length identified within the pure Zn_6O_6 cluster was 2.01 Å similar to the work done by Wang et al. [17]. Replacing one of the Zinc atoms in the pure Zn_6O_6 nanocluster by Ni atom results the deformation in the bond length of Ni–O, Zn–O bonds are observed at 2.0 Å and 1.93 Å, respectively.

The Acrolein comprises of three possible interaction sites for the adsorption with $NiZn_5O_6$. The functionalization of Acrolein on $NiZn_5O_6$ cluster considered for three possible interaction sites with the functional groups of the = O Carbonyl group (C), –CH Methyl group (M_1), and –CH_2 Methylene group (M_2). The intercommunication of $NiZn_5O_6$ with Acrolein at three sites are seen in Figure 2.

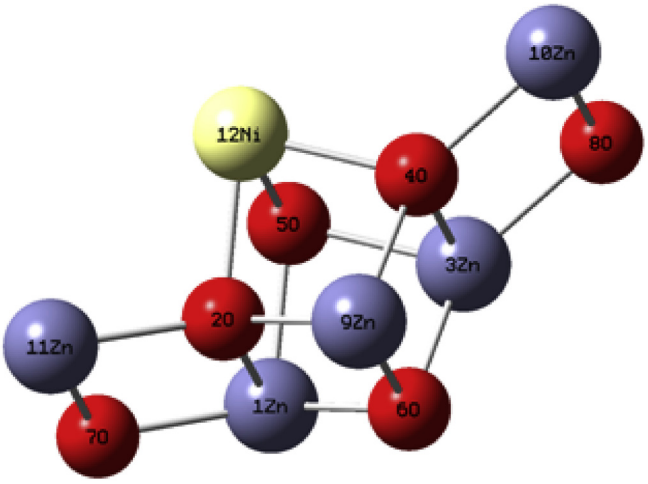

Figure 1. Optimized structure of $NiZn_5O_6$ calculated at B3LYP/6-31G level of theory.

The substitution of Ni at the 12th position of Zn in $NiZn_5O_6$ nanocluster for the three interaction sites exhibits the deformation in the Zn–O bond length of 1.86Å, 1.98Å, and 1.89 Å, respectively. The big difference in bond distance is observed at Zn(5)–O(7) and Zn(5)–O(4) in the C site of A-$NiZn_5O_6$ cluster. The bond distance of Ni–O is decreased to 1.91Å in C site. The big difference in bond distance was observed at Zn(5)–O(9), Zn(2)–O(7) and Zn(5)–O(4) in the M_1 site. The bond distance of Ni–O at the M_1 interaction site was observed as 2.0Å. The higher the difference in bond length was found at Zn (2) –O(7), Zn(5)–O(7) and O(4)–Zn(5) for the M_2 site. The bond length of the Ni–O bond was observed as 1.9Å in the M_2 site. The bond angle varies from 60° to 147° when Acrolein interacting with the $NiZn_5O_6$ cluster through the Ni atom. The greater bond angle difference between $NiZn_5O_6$ and A-$NiZn_5O_6$ was observed at an angle O(7)-Zn(8)-O(11), Zn(5)-O(9)-Zn(10) and Zn(10)-O(9)-Ni(12) for C site. The lower bond length of the C site of A- $NiZn_5O_6$ correlated with the excessive binding energy, which associated with the chemisorption mechanism [18].

The adsorption energies (E_{ad}) of C, M_1 and M_2 sites of Acrolein on $NiZn_5O_6$ via Ni atom are calculated as -2.73 eV, -1.04 eV, -0.89 eV respectively. The E_{ad} of Acrolein on the surface of $NiZn_5O_6$ through Zn atom and O atom are found to be less as compared to Ni atom and hence the interaction of Acrolein on $NiZn_5O_6$ through Ni atom is scrutinized in this manuscript. The E_{ad} of Acrolein on $NiZn_5O_6$ via Zn atom is calculated to be -0.72 eV and via O atom is found to be -0.09 eV. The structural data consists of bond length and bond angle were listed in Table 1 and Table 2. The negative adsorption energy of the Acrolein molecule on $NiZn_5O_6$ is the characteristic of the chemisorption mechanism [19].

3.2. Frontier molecular orbital analysis

Figure 3 shows the spatial orientation of the frontier orbitals HOMO and LUMO, obtained by the density Functional Theory to analyze the positioning of the orbitals is revealed that the degree of HOMO density is located in the dopant atom Ni and the significant parts of the A- $NiZn_5O_6$ in relation to the LUMO this concentration stops at Acrolein molecule not including the methyl, methylene and carbonyl groups, these data are chemical- descriptors quantum play an important role in chemical reactions and the formation of several charge transfer complex. The orbital HOMO (Highest Occupied Molecular Orbital) measures the electron-donor character of A- $NiZn_5O_6$ specified by green color and the LUMO (Lowest Unoccupied Molecular Orbital) measures the electron-acceptor

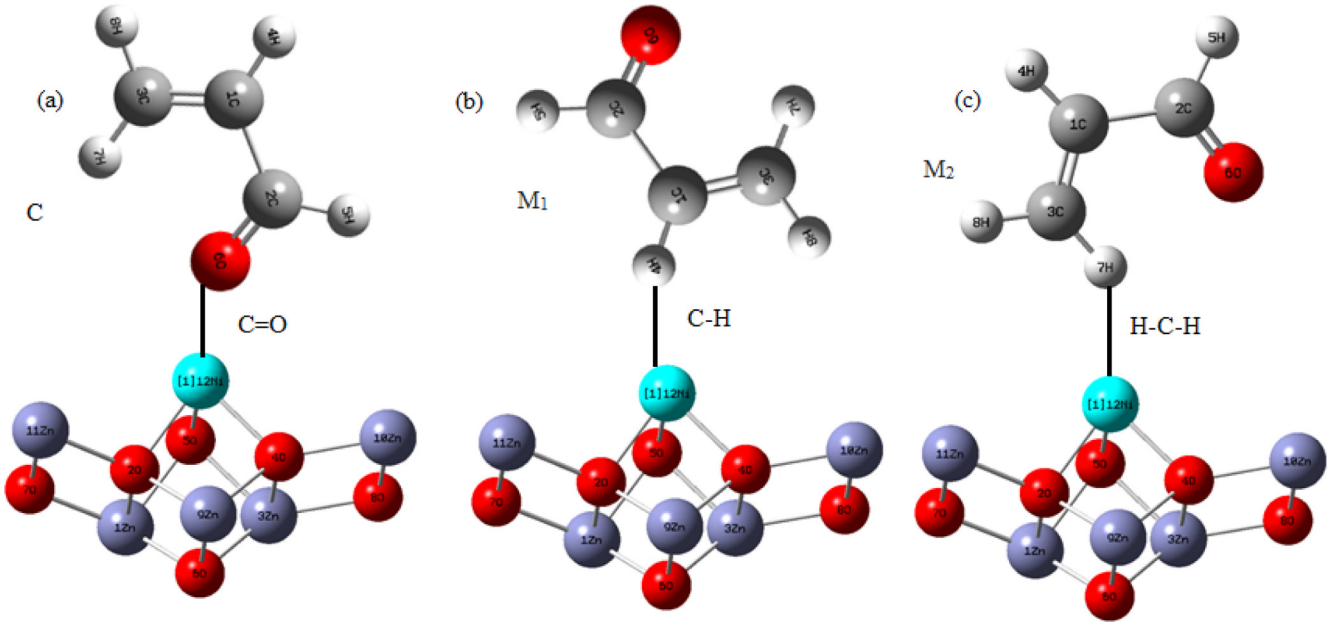

Figure 2. The adsorption of acrolein on Ni doped Zn_6 O_6 with (a) C (Carbonyl) (b) M_1 (Methyl) (c) M_2 (Methylene) interaction site calculated at B3LYP/6-31G level of theory.

character specified by red color. From these definitions, it is observed that the higher the energy of the HOMO greater electrondonating ability, and the lower the energy of the LUMO is less resistance to accept electrons. The energies of the HOMO and LUMO are used as chemical reactivity indices and are commonly correlated with other indices, such as electron affinity and ionization potential.

Table 1. The calculated bond length of $NiZn_5O_6$, C, M_1, M_2 interaction site of A-$NiZn_5O_6$ at B3LYP/6-31G level of theory in the ground state analysis.

Bond distance	NiZn5O6	C	M_1	M_2
Zn(1)-O(2)	1.934	1.861	1.983	1.901
O(5)-Zn(1)	1.929	1.861	1.982	1.903
Zn(1)-O(6)	1.931	1.852	1.985	1.892
Zn(1)-O(7)	1.927	1.853	1.987	1.893
Zn(9)-O(2)	1.922	1.871	1.991	1.916
Zn(11)-O(2)	1.932	1.864	1.983	1.902
O(6)-Zn(9)	1.939	1.839	1.988	1.925
O(2)-Ni(12)	2.032	1.912	2.028	1.999
Zn(3)-O(4)	1.927	1.849	1.985	1.945
Zn(3)-O(5)	1.926	1.864	1.971	1.902
O(6)-Zn(3)	1.939	1.861	1.966	1.903
O(4)-Ni(12)	2.003	1.913	2.014	1.998
O(4)-Zn(9)	1.929	1.851	1.982	1.906
Zn(10)-O(4)	1.936	1.866	1.988	1.909
Zn(11)-O(7)	1.935	1.862	1.987	1.908
O(8)-Zn(10)	1.938	1.868	1.982	1.901
O(5)-Ni(12)	2.007	1.919	1.999	1.994
Ni(12)-O(18)	-	1.738	-	-
Ni(12)-H(16)	-	-	1.439	-
Ni(12)-H(20)	-	-	-	1.091
C(13)-C(14)	-	1.54	1.542	1.544
C(13)-H(16)	-	1.09	1.092	1.101
C(14)-H(17)	-	1.096	1.106	1.093
C(13)-C(15)	-	1.387	1.441	1.432
C(14)-O(18)	-	1.43	1.432	1.436
C(15)-H(19)	-	1.092	1.096	1.099
C(15)-H(20)	-	1.094	1.091	1.101

The HOMO and LUMO distributions of $NiZn_5O_6$ and three sites of A-$NiZn_5O_6$ computed using B3LYP/6-31G (d,p) level are shown in Figure 3. The Zn_6O_6 nanocluster is a broad bandgap semiconductor material. Nickel is a metal with an E_g of 0.22 eV. In the $NiZn_5O_6$ system, the HOMO and LUMO are located around the Ni atom implying that the Ni doping causes the formation of new energy levels nearer to the Fermi level. The energies of HOMO and LUMO of $NiZn_5O_6$ are -5.83 and -2.94 eV with E_g of 2.89 eV. The functionalizing compound Acrolein has a high E_g of 4.80 eV. Acrolein is introduced on the uppermost layer of $NiZn_5O_6$ and interacts via Ni atom to modify its electrical properties caused by the changes in molecular orbitals concerning their densities and energies. Upon adsorption of Acrolein, remarkable changes are observed for HOMO and LUMO distributions of A- $NiZn_5O_6$. The E_{HOMO} and E_{LUMO} of C, M_1 and M_2 sites of A-$NiZn_5O_6$ are -4.98, -3.86, -5.74, -2.99, -4.82 and -3.05 eV respectively. The E_g of the three sites are 1.12, 2.75, and 1.77 eV. In the C and M_2 interaction site of A- $NiZn_5O_6$ system, the HOMO is mainly localized on the Ni center while LUMO is on the ZnO substrate which corresponds to the changes in their relative energies. The HOMO and LUMO of the M_1 site of A-$NiZn_5O_6$ is situated on the acceptor end of the material. Acrolein adsorption increases the E_{HOMO} and decreases the E_{LUMO} of $NiZn_5O_6$. Interaction of Acrolein causes a decrement in bandgap which gives lower kinetic stability, larger electron conductivity and higher chemical reactivity make the compound to be potentially used in photovoltaic applications [20]. The photovoltaic properties were investigated for A-$NiZn_5O_6$ as a donor with PCBM as an acceptor in dye-sensitized solar cells concerning the extraordinary property of ZnO nanomaterial as a shallow donor or acceptor [20]. The E_{HOMO} and E_{LUMO} energies of PCBM were calculated as -6.10 eV and -3.70 eV. The LUMO magnitude of the compound A-$NiZn_5O_6$ at all the sites was more elevated than the HOMO magnitude of PCBM. The HOMO/LUMO energy, E_g, adsorption energy (E_{ad}) and ΔE_g of A-$NiZn_5O_6$ were tabulated in Table 3. By repeating all the computations by B3LYP/6-31G, B3LYP/6-311G and B3LYP/LanL2DZ level of theory, the E_g was larger than it was computed by B3LYP/6-31G.

The Acrolein decoration on $NiZn_5O_6$ causes a significant transposition of the occupied orbital to higher energy levels existed in the

middle of HOMO and LUMO of the $NiZn_5O_6$ cluster. The HOMO is extremely switched on higher energy levels, but LUMO is hardly shifted to lower energy levels. Therefore, electrons in the donor consecutively shifted to the acceptor of the dye molecule and then the electrons are injected into the occupied state of PCBM after photons were incident on A-$NiZn_5O_6$. The calculated band gap of the three sites of A-$NiZn_5O_6$ is increased in the order C > M_1>M_2. The open-circuit voltage of dye-sensitized solar cells has been linearly related to the filled state of the donor and the unfilled state of the acceptor [21]. The value of Voc is obtained using gas phase calculations based on the geometry optimized with PCBM. The theoretical value of open-circuit voltage V_{OC} of the solar cell is calculated by,

$$V_{OC} = |E_{HOMO}\ (Donor)| - |E_{LUMO}\ (Acceptor)| - 0.3 \quad (2)$$

Where, the value 0.3V is an empirical factor. The calculated Voc of C site of A-$NiZn_5O_6$ is 3.41eV while the values of M_1 and M_2 site are 3.35 and 2.54 eV, respectively. These values of V_{OC} are sufficient for efficient electron injection into LUMO of the acceptor. The nanocomposite A-$NiZn_6O_6$ is an efficient photosensitizer on account of its good light absorption characteristics. The decrement in the E_g of A-$NiZn_6O_6$ can harvest more light it assists the higher short-circuit current density (Jsc) [22].

Table 2. The calculated bond angle of $NiZn_5O_6$, C, M_1, M_2 interaction site of A-$NiZn_5O_6$ at B3LYP/6-31G level of theory in the ground state analysis.

Bond Angle	$NiZn_5O_6$	C	M_1	M_2
Zn(2)-O(1)-Zn(3)	92.3	85.9	95.3	88.1
O(1)-Zn(2)-O(4)	87.5	80.5	90.9	83.2
O(1)-Zn(2)-O(6)	127.1	119.4	131.2	121.4
O(1)-Zn(2)-O(7)	118.8	111.5	121.2	114.7
O(4)-Zn(2)-O(6)	62.1	59.34	65.3	62.9
O(6)-Zn(2)-O(7)	71.2	68.8	75.9	71.9
O(1)-Zn(3)-O(4)	87.3	81.9	91.3	84.5
Zn(2)-O(4)-Zn(3)	92.5	88.5	95.2	91.2
Zn(2)-O(4)-Zn(5)	135.3	129.6	138.7	131.2
Zn(2)-O(4)-Ni(12)	117.3	109.6	121.2	112.8
Zn(3)-O(4)-Zn(5)	120.8	112.3	125.2	115.4
Zn(3)-O(4)-Ni(12)	122.8	117.5	127.3	120.2
O(4)-Zn(5)-O(9)	103.9	97.6	109.5	100.9
O(7)-Zn(5)-O(9)	99	91.5	104.2	94.4
Zn(2)-O(6)-Zn(8)	104.9	97.5	110.3	100.1
Zn(2)-O(6)-Ni(12)	118.2	112	121.2	124.4
Zn(2)-O(7)-Zn(5)	132.3	128.3	136.7	139.6
Zn(2)-O(7)-Zn(8)	103.7	97.5	106.8	100.3
Zn(5)-O(7)-Zn(8)	79.8	71.1	84.2	74.3
O(6)-Zn(8)-O(7)	71.3	66.9	78.5	69.4
O(6)-Zn(8)-O(9)	109.7	101.4	115.4	104.6
O(6)-Zn(8)-O(11)	131.9	128.3	136.3	131.5
O(7)-Zn(8)-O(9)	100.1	93.2	106.3	96.2
O(7)-Zn(8)-O(11)	147.1	139.4	151.5	142.3
O(9)-Zn(8)-O(11)	92.78	84.5	94.5	87.5
Zn(5)-O(9)-Zn(8)	80.8	74.3	86.3	77.4
Zn(5)-O(9)-Zn(10)	140.7	133.8	146.9	136.8
Zn(8)-O(9)-Zn(10)	86.66	80.5	92.5	83.5
Zn(10)-O(9)-Ni(12)	137.6	130.7	142.8	133.5
O(9)-Zn(10)-O(11)	93.3	85.9	99.6	102.7
Zn(8)-O(11)-Zn(10)	86.6	79.1	92.3	95.3
O(4)-Ni(12)O(6)	62.1	56.7	71.3	59.4
C(15)-C(14)-H(18)		128.7	132.7	130.2
C(14)-C(15)-O(19)		124.8	128.8	126.3
C(14)-C(15)-H(20)		89.6	93.6	91.2
C(19)-C(15)-H(20)		128.1	131.8	130.5

3.3. Anchoring group effects on the IPCE

The short-circuit current density (Jsc) is closely connected to the charge conversion efficiency (η) of the solar cell is defined as,

$$Jsc = \int LHE\ (\lambda)\ \varphi_{Inject}.\eta_{collect}\ d\lambda \quad (3)$$

Where LHE (λ) is the light harvesting efficiency, φ_{Inject} is the electron injection potency and $\eta_{collect}$ is the electron collection efficiency.

The large φ_{Inject} leads to higher short circuit current density (Jsc). The φ_{Inject} is analogous to the driving force of the electron inoculation (ΔG^{inject}) from the photoinduced excited state of A-$NiZn_6O_6$ on the semiconductor surface and φ_{Inject} is directly proportional to the free energy of electron injected as

$$\varphi_{Inject}\ \alpha\ f\ (-\ \Delta G^{inject}) \quad (4)$$

$$\Delta G^{Inject} = E^{dye*} - E_{CB} \quad (5)$$

Where E^{dye*} is the oxidative potential energy in the excited state and E_{CB} represents the reduction potential of the conduction band. E^{dye*} can be estimated by,

$$E^{dye*} = E^{dye} - \Delta E \quad (6)$$

Where E_{dye} represents the energy of oxidation potential in the ground state and ΔE is the energy of electronic vertical transition corresponding to λ_{max}.

3.4. Spectral analysis

The wavelength (λ), excitation energy (ΔE), oscillator strength (f) and light harvesting efficiency (LHE) were computed using singlet excited state at the B3LYP/6-31G++(d,p) functional using the time-dependent density functional theory (TD-DFT) calculations. The π conjugate element A-$NiZn_5O_6$ is beneficial in decreasing the E_g and increasing the light harvesting ability. The lowest singlet to singlet excited state transition was investigated to enumerate the electronic absorption mechanism in whole visible/near-IR regions. The A-$NiZn_6O_6$ composite showed the broad absorption of photons in the visible region and the electronic excitations were observed to be π – π* transitions. The absorption bands λ_{max} of $NiZn_5O_6$ and the three configurations of A-$NiZn_5O_6$ were observed at 511, 545, 448, and 459 nm respectively. The LHE can be expressed as [23]

$$LHE = 1\text{-}10^{-f} \quad (7)$$

Where, f is the oscillator strength of the absorption spectra of A-$NiZn_6O_6$. The highest oscillator strength of 13.8 is linked to the C site of A-$NiZn_5O_6$ in 545 nm wavelength while the modest value of oscillator strength 0.61 belongs to the M_2 site of A-$NiZn_5O_6$ in 441 nm. Thus, the C site of A-$NiZn_5O_6$ shows a good light response.

3.5. Density of states

The correlation between the electrical conductivity and the E_g can be illustrated by,

$$\sigma\ \infty\ \exp\ (E_g / kT) \quad (8)$$

Where σ is the electrical conductivity and k is the Boltzmann constant. As the conductivity was exponentially associated with the negative rate of the bandgap, conductivity became huge as E_g was declined [24]. This equation commonly utilized to examine the sensitivity of nanostructured A-$NiZn_5O_6$. Figure 4 exhibits the DOS plots of $NiZn_5O_6$, C, M_1 and M_2 sites of A-$NiZn_5O_6$. The Fermi energy of $NiZn_5O_6$ is -4.38 eV. The Fermi energy of the C site of A-$NiZn_5O_6$ is calculated as -4.42 eV. The reduction in Fermi energy of the C site of A- $NiZn_5O_6$ specifies the Fermi level shifted to the valence band, which intensifies the work function. This

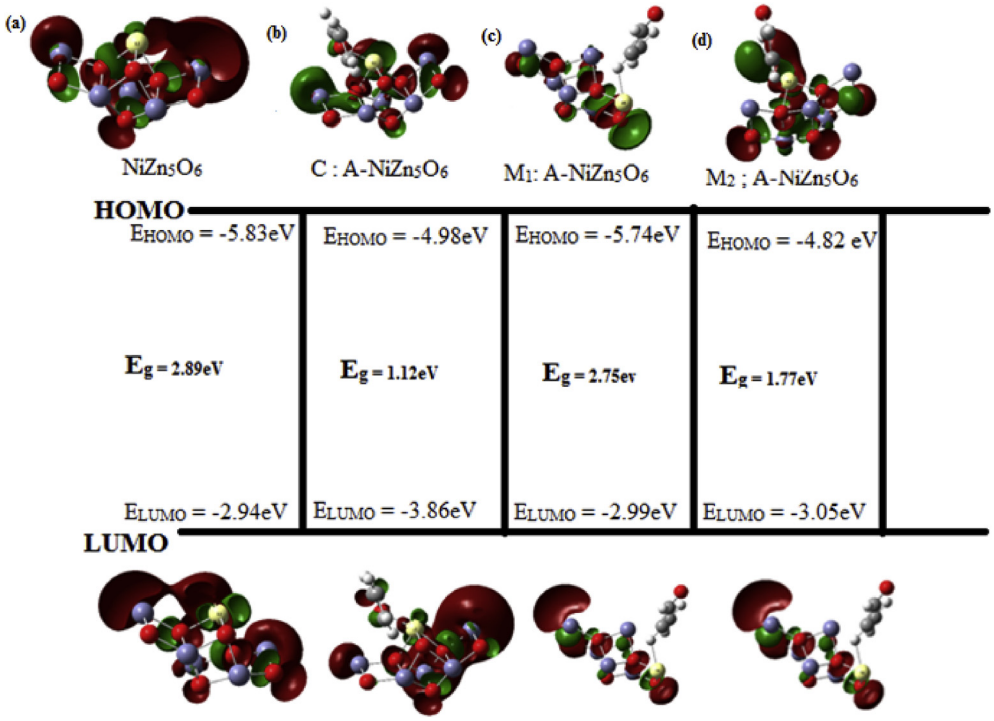

Figure 3. The HOMO/LUMO pictures of (a) $NiZn_5O_6$ (b) C interaction site of A-$NiZn_5O_6$ (c) M_1 interaction site of A-NiZn5O6 (d) M_2 interaction site of A-$NiZn_5O_6$.

stimulating phenomenon makes A-$NiZn_5O_6$ composite detects uses in field emission properties [25].

3.6. Global reactivity descriptors

The global indices of reactivity are determined from the HOMO and LUMO energies of A-$NiZn_6O_6$. The E_g had wider importance in understanding the static molecular reactivity and helps in characterizing the kinetic stability of A-$NiZn_5O_6$. The small-scale energy gap material is highly polarizable and causes the ease of transporting electrons. The reactive descriptors such as the ionization potential (IP), electron affinity (EA), electronegativity (χ), hardness (η), softness (S), chemical potential (μ), electrophilicity index (ω), charge transfer (ΔNmax), nucleofugality (ΔEn) and electrofugality (ΔEe) of $NiZn_5O_6$ and A-$NiZn_5O_6$ are computed by DFT/6-31G++g(d,p) and presented in Table 4.

From Koopman's theorem,

The ionization potential and electron affinity are,

$$I = -E_{HOMO};\ A = -E_{LUMO} \tag{9}$$

The prohibitive ionization energy at the M_1 site indicates higher stability. The declined ionization energy at the M_2 site indicates higher reactivity [26]. The reactivity of A-$NiZn_5O_6$ was determined through chemical hardness, chemical softness, electronegativity, and electrophilicity index. The chemical hardness of the A-$NiZn_5O_6$ was principally calculated as,

$$\eta = (E_{LUMO} - E_{HOMO})/2 \tag{10}$$

The softness can be determined as follows,

$$S = 1/2\eta \tag{11}$$

The chemical hardness and softness are the salient properties to quantify the molecular stability and reactivity [27]. The softness of A-$NiZn_5O_6$ at three sites is calculated as 0.892 eV, 0.364, and 0.568 eV respectively. The hardness of the three sites is 0.56, 1.37 and 0.88 eV respectively. The above values predicted that the hardness and softness are reciprocal to one another. It can be observed that the conversion efficiency increases while the chemical hardness decreases. The small-scale hardness of the C site proposed as the best candidate for intramolecular charge transfer and higher short-circuit current density (Jsc). The order of chemical hardness was C < M_2 < M_1

The electrophilicity index values are calculated by the equation,

$$\omega = \mu^2/2\eta \tag{12}$$

$$\omega^{+} = (I+3A)^2/16(I-A) \tag{13}$$

Parr *et.al* has analyzed the electrophilicity index (ω) describes the chemical reactivity of Acrolein with $NiZn_5O_6$ [28]. The electron

Table 3. The values of HOMO and LUMO energies(E_{HOMO} and E_{LUMO}), energy Gap (E_g) and Fermi energy (E_F) of $NiZn_5O_6$, C, M_1, M_2 interaction site of A-$NiZn_5O_6$ calculated at B3LYP/6-311G, 6-31G and the LANL2DZ level of theory.

System	Method	E_{HOMO} eV	E_F eV	E_{LUMO} eV	E_g eV	$^b\Delta E_g$ eV
$NiZn_5O_6$	B3LYP/6-31G	-5.83	-4.38	-2.94	2.89	-
C		-4.98	-4.42	-3.86	1.12	1.77
M_1		-5.74	-4.36	-2.99	2.75	0.14
M_2		-4.82	-3.93	-3.05	1.77	1.12
$NiZn_5O_6$	B3LYP/6-311G	-5.92	-4.31	-2.71	3.21	-
C		-4.83	-4.26	-3.69	1.14	2.07
M_1		-5.8	-4.27	-2.74	3.06	0.15
M_2		-4.75	-3.78	-2.81	1.94	1.27
$NiZn_5O_6$	B3LYP/LANL2DZ	-5.9	-4.34	-2.79	3.11	-
C		-4.68	-4.1	-3.52	1.16	1.95
M_1		-5.84	-4.37	-2.9	2.94	0.17
M_2		-4.65	-3.74	-2.84	1.81	1.3
PCBM	B3LYP/6-31G	-6.1	-4.9	-3.7	2.4	0.49

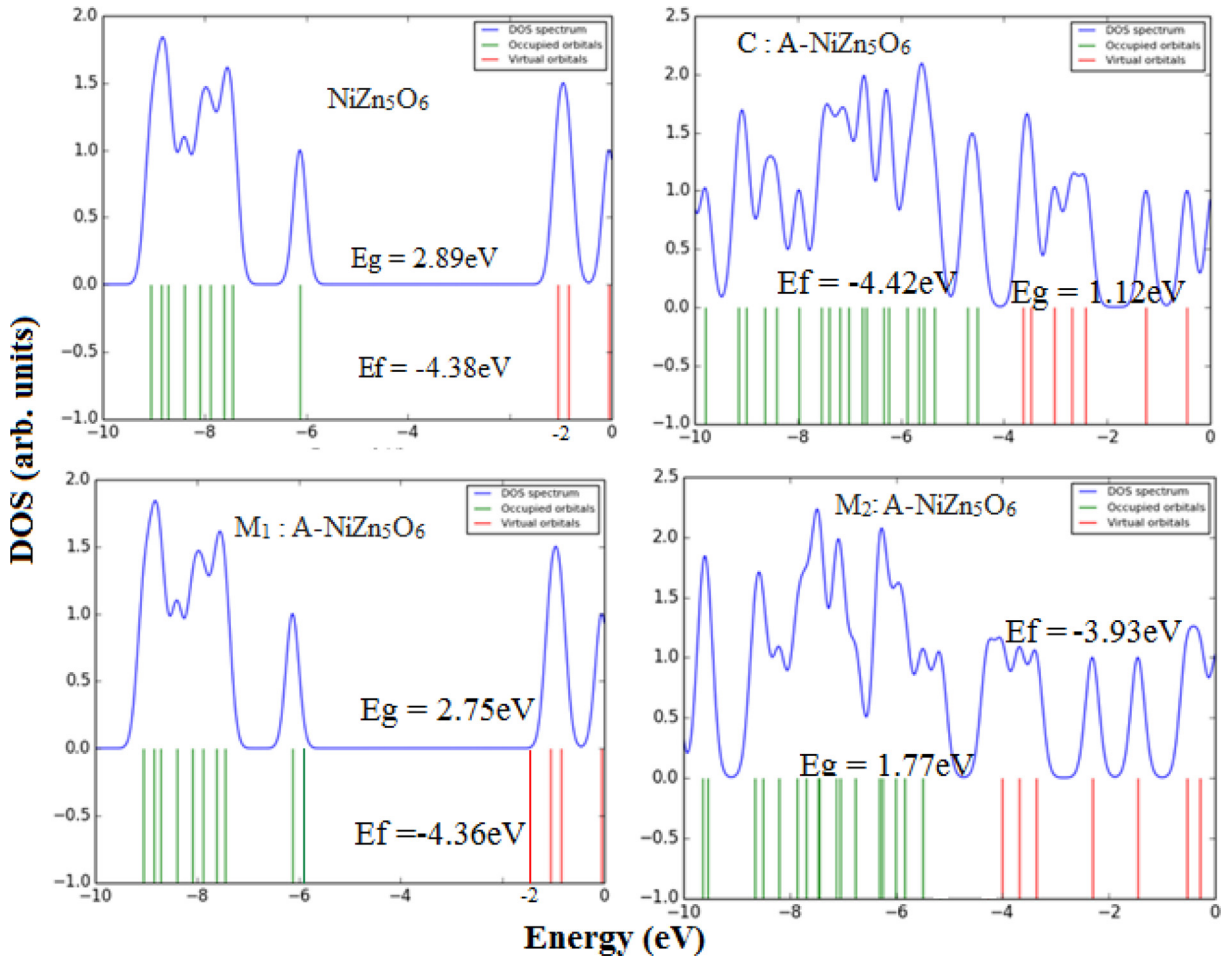

Figure 4. The DOS plot of (a) $NiZn_5O_6$ (b) C interaction site of A-$NiZn_5O_6$ (c) M_1 interaction site of A-$NiZn_5O_6$ (d) M_2 interaction site of A-$NiZn_5O_6$.

accepting the power of A-$NiZn_5O_6$ was calculated by the Eq. (9). The C site of A-$NiZn_5O_6$ had the highest ω^+ value of 15.3 eV. Thus, the C site of A-$NiZn_5O_6$ had the largest ability to accept electrons towards the acceptor part of A-$NiZn_5O_6$. The values of ω^+ were in the order C > M_2> M_1. The present study indicated that the lower chemical hardness, the higher electron accepting power, the better short-circuit current density of the C site consequently had a better light conversion efficiency.

The M_1 site of the nucleophile, A-$NiZn_5O_6$ had an electrophilicity index **(ω)** of 6.93 eV in opposite an electrophile C site had an electrophilicity index (ω) of 17.44 eV. The global electrophilicity index assesses the stabilization in energy when the nanocomposite A-$NiZn_5O_6$ gains an added charge ΔN from the surroundings [29].

Table 4. Global Reactivity Descriptors, dipole moment, mean polarizability and total static hyperpolarizability of $NiZn_5O_6$, C, M_1, M_2 interaction site of A-$NiZn_5O_6$ calculated at the B3LYP/6-31G level of theory.

Property	$NiZn_5O_6$	C: A- $NiZn_5O_6$	M_1: A- $NiZn_5O_6$	M_2: A- $NiZn_5O_6$
$I = -E_h$ eV	5.83	4.98	5.74	4.82
$A = -E_l$ eV	2.94	3.86	2.99	3.05
$\eta = (I - A)/2$eV	1.44	0.56	1.37	0.88
$\mu = -(I + A)/2$	-4.38	-4.42	-4.36	-3.93
$\Psi = -\mu$	4.38	4.42	4.36	3.93
$S = 1/2\eta$eV	0.347	0.892	0.364	0.568
$\omega = \mu^2/2\eta$eV	6.66	17.44	6.93	8.77
$\Delta Nmax = -\mu/\eta$	3.04	7.89	3.18	4.46
$\Delta E_n = A+\omega$	9.6	21.3	9.92	11.82
$\Delta Ee = I+\omega$	12.49	22.42	12.67	13.59
Polarizability	-113	-131.35	-135.9	-139.97
Hyperpolarizability	22.87	37.03	39.58	154.07
Dipole Moment	7.16	6.52	13.16	7.08

$$\Delta N_{max} = -\mu/\eta \quad (14)$$

The nucleofugality (ΔEn) and electrofugality (ΔEe) are [30, 31],

$$\Delta E_n = EA+\omega = (\mu+\eta)^2/2\eta \quad (15)$$

$$\Delta E_e = IP+\omega = (\mu-\eta)^2/2\eta \quad (16)$$

The chemical potential of A-$NiZn_5O_6$ at various basis sets are calculated by,

$$\mu = -(E_{LUMO} + E_{HOMO})/2 \quad (17)$$

The chemical potential of the M_2 site of A-$NiZn_5O_6$ was higher than the other sites with the value -3.93 eV. The electronegativity of the A-$NiZn_5O_6$ composite is the negative of chemical potential. The chemical potential is analogous to the electronegativity. The chemical potential and the Fermi level of A-$NiZn_5O_6$ are calculated at the center point of the E_g and hence the chemical potential is indistinguishable with the Fermi level of A-$NiZn_5O_6$.

3.7. Mulliken population analysis

The Mulliken atomic charges of $NiZn_5O_6$ and A-$NiZn_5O_6$ of three various interaction sites were listed in Table 5. The investigation of Mulliken charges of each atom in $NiZn_5O_3$ and A-$NiZn_5O_6$ employs DFT/B3LYP functional with a 6-31G++(d, p) basis set [32]. The Mulliken charge plot appeared in Figure 5. In the $NiZn_5O_6$ configuration, the atoms Zn_2, Zn_3, Zn_5, Zn_8, Zn_{10}, and Ni_{12} possess positive charges, which are

Table 5. Mulliken atomic charges of $NiZn_5O_6$, C, M_1, M_2 interaction site of A-$NiZn_5O_6$ calculated at B3LYP/6-31G level of theory.

Atom	NiZn5O6	C:A-NiZn5O6	M_1:A-NiZn5O6	M_2:A-NiZn5O6
O1	-0.718	-0.731	-0.706	-0.721
Zn2	0.955	0.933	0.94	0.922
Zn3	0.463	0.576	0.575	0.483
O4	-0.625	-0.624	-0.635	-0.615
Zn5	0.711	0.761	0.905	0.754
O6	-0.685	-0.726	-0.735	-0.717
O7	-0.521	-0.534	-0.508	-0.52
Zn8	0.598	0.691	0.648	0.685
O9	-0.832	-0.841	-0.821	-0.836
Zn10	0.69	0.711	0.694	0.701
O11	-0.664	-0.688	-0.664	-0.678
Ni12	0.63	0.483	0.243	0.471
C13		-0.436	-0.303	-0.42
C14		-0.127	-0.299	-0.09
C15		0.234	0.246	0.227
H16		0.236	0.209	0.226
H17		0.227	0.141	0.217
H18		0.218	0.315	0.201
O19		-0.452	-0.41	-0.441
H20		0.167	0.165	0.15

acceptors. The atoms O_1, O_2, O_3, O_4, O_5, and O_6 have negative charges, which are donors. The Oxygen O_9 was more negative of -0.832e. The Zn_2 atom shows a more positive charge of the value 0.955e. In the C site of A-$NiZn_5O_6$, the atoms Zn_2, Zn_3, Zn_5, Zn_8, Zn_{10}, Ni_{12}, C_{15}, H_{16}, H_{17}, H_{18}, and H_{20} have positive charges that are acceptors. The atoms O_1, O_4, O_6, O_7, O_9, O_{11}, C_{13}, C_{14}, and O_{19} have negative charges that are donors. The Oxygen O_9 was more negative of -0.841e. The Zn_2 atom has a more positive charge of 0.955e.

3.8. Molecular electrostatic potential (MEP), dipole moment and polarizability analysis

The MEP was figured out to investigate the interactions and charge distributions of $NiZn_5O_6$ and the A-$NiZn_5O_6$ complex. The MEP is a wonderful practice to envision the polarity of the individual atom present in the sensitizer compound. All isosurfaces are illustrated by the iso-value of 0.0004 e/au^3 in the Gauss View program. The MEP surface prompted using the charge assignments of the nanocomposite at an atomic site is defined as,

$$V(r) = \sum \frac{z_A}{[R_A - r]} - \int \frac{\rho(r')dr'}{|r - r'|} \quad (18)$$

Where, Z_A is the charge on the nucleus A at R_A [33]. The electrostatic potential maps of $NiZn_5O_6$ and A-$NiZn_5O_6$ were presented in Figure 6. The MEP framework in Figure 6a shows that the Zn atoms and Ni atom were positively charged (blue in color) while the O atoms were negatively charged (red in color) because there was the charge shifted from Zn atoms and Ni atom to the O atoms predicting ionic bonds in the $NiZn_5O_6$ surface. Figure 6b–d show that the sector of Zn atoms was identified by the red colour, specify the negative charge because there is the charge shifted from the Acrolein molecule to $NiZn_5O_6$.

The dipole moment and polarizability are useful parameters of dyes in solar cells. The dipole moment (μ) of $NiZn_5O_6$, A-$NiZn_5O_6$ at three sites and Acrolein were estimated at 7.16, 6.52, 13.16, 7.08 and 2.97 Debye. The dipole moment of C and M_2 geometries were more intense than the M_1 geometry. The highest deformation was observed when Acrolein decorated on the C interaction site of $NiZn_5O_6$ nanocluster. The dipole moment vector and binding energy have an inverse relationship with one another. This inverse relationship can be explained by the distance of Acrolein from the $NiZn_5O_6$ nanocluster. The larger bond length of $NiZn_5O_6$ to Acrolein predicts the lowest binding energy causes a larger dipole moment. The lower bond distance of the C site of A-$NiZn_5O_6$ predicts larger adsorption energy causes smaller dipole moment.

The polarizability (α) and the total first static hyperpolarizability (β) of $NiZn_5O_6$ and A- $NiZn_5O_6$ for all the orientations were enumerated by DFT using B3LYP/6-31G++(d.p) basis set. The first static hyperpolarizability can be narrated by the 3 × 3 × 3 matrix. The 27 constituents of the matrix declined to 10 components due to Kleinman symmetry [34].

The polarizability (α) and total first static hyperpolarizability (β) using x, y, z coordinates can be denoted by,

The isotropic polarizability, $(\alpha) = [\alpha_{xx}+\alpha_{yy}+\alpha_{zz}]/3$ and the average hyperpolarizability is,

$$\beta_{TOTAL} = (\beta_x^2+\beta_y^2+\beta_z^2)^{1/2} \quad (19)$$

$$= [(\beta_{xxx}+\beta_{xyy}+\beta_{xzz})^2+(\beta_{yyy}+\beta_{yxx}+\beta_{yzz})^2+(\beta_{zzz}+\beta_{zxx}+\beta_{zyy})^2]^{1/2} \quad (20)$$

The mean polarizability (α) and total static hyperpolarizability (β) of $NiZn_5O_6$ and A-$NiZn_5O_6$ were collected in Table 4. The isotropic polarizability of A-$NiZn_5O_6$ was decreased as compared to the $NiZn_5O_6$ cluster. The β_{xyy} and β_{xzz} components subscribe to a huge part of hyperpolarizability in A-$NiZn_5O_6$. The β_{yzz} and β_{xyz} components donate a large part of hyperpolarizability in $NiZn_5O_6$.

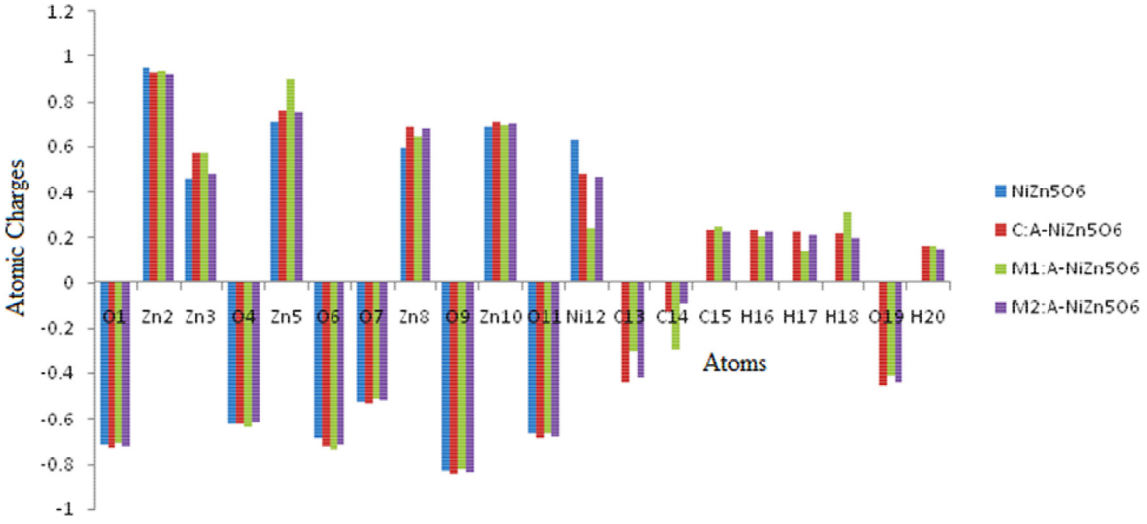

Figure 5. Mulliken atomic charge plot of $NiZn_5O_6$ and C, M_1, M_2 interaction sites of A-$NiZn_5O_6$ calculated at B3LYP/6-31G level of theory.

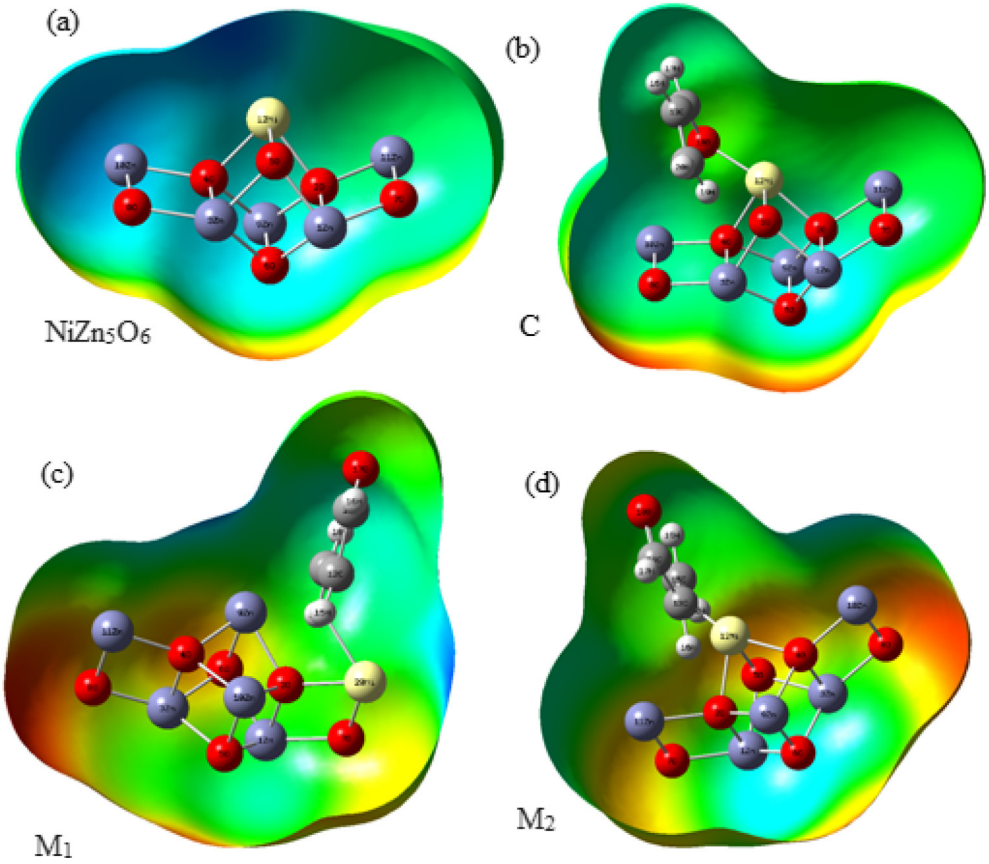

Figure 6. Molecular electrostatic potential surfaces for (a) $NiZn_5O_6$ (b) C interaction site of A-$NiZn_5O_6$ (c) M_1 interaction site of A-$NiZn_5O_6$ (d) M_2 interaction site of A-$NiZn_5O_6$ calculated at B3LYP/6-31G level of theory.

3.9. Vibrational analysis

The IR frequencies also furnish the confirmation of the existence of powerful synergy between the Acrolein molecule and $NiZn_5O_6$. Assignments that involve $NiZn_5O_6$ cluster coordinates in the Acrolein molecule of C1 symmetry are based strictly on the DFT, B3LYP/6-311G (d,p) analysis. There are 30 possible modes of vibrations that were present in the $NiZn_6O_6$. The absorption peaks at 430cm^{-1} and 547cm^{-1} have corresponded to the Zn–O stretching vibrations in a simulated IR spectrum of $NiZn_5O_6$. The stretching vibration of Ni–O was observed in 451cm^{-1}. In the theoretical spectrum of A-$NiZn_5O_6$, C=O stretching is found in the region of 1863cm^{-1}. In previous work, the frequency of C–C stretching vibration of Acrolein has been reported as 1158cm^{-1} [35, 36]. In the geometrical parameters of A-$NiZn_5O_6$, the band 1007 cm^{-1} assigned to C–C stretching vibration with strong intensity. The two higher wavenumbers 2987cm^{-1} and 2934cm^{-1} were assigned to the C–H stretching with strong intensity. The weak C–H stretching vibration was assigned to 3020cm^{-1} and 3054cm^{-1}. In the spectral region of 1530–1420 cm^{-1} infrared band was assigned to HCH vibrational modes. Furthermore, a Zn–O stretching mode of A- NiZn5O6 was shifted towards the higher wavenumber region as compared to $NiZn_5O_6$. The mode calculated at 1546cm^{-1} assigned to C=C stretching with strong intensity.

4. Conclusion

The computational investigation of $NiZn_5O_6$, C, M_1 and M_2 sites of A- $NiZn_5O_6$ have been studied to determine their potential efficiency in solar cells compared with the anchoring group PCBM. The molecular geometries, E_g, and HOMO and LUMO densities have been evaluated using DFT calculations for four new dyes. The excitation energies, absorption properties such as maximum wavelength, oscillator strength and the light harvesting efficiency of dyes have also been studied by TD-DFT calculations. The anchoring properties of the dyes and the potency of electron injection were investigated by the evaluation of polarizabilities. The C interaction site of A-$NiZn_5O_6$ with a small band gap built it a promising nanocomposite in photovoltaic applications than other dyes. The chemical reactivity parameters such as electrophilicity, chemical hardness, and electron accepting power proved that the C site of A-$NiZn_5O_6$ has high conversion efficiency. Absorption over a wide range of wavelengths due to the intramolecular π-π^* interaction, extending into the near-IR region due to a small HOMO-LUMO energy gap proved that the C site is harvesting a large fraction of the solar spectrum, which in turn produces a high photocurrent and thus highly efficient solar cell performance than M_1 and M_2 dyes. Our results strongly suggest that the A-$NiZn_5O_6$ dyes can be successfully designed for use in DSSCs and further demonstrate the promising performance of DSSCs based on dye sensitizers. We believe that our results may provide basic guidelines for further theoretical and experimental study.

Declarations

Author contribution statement

S. Dheivamalar: Conceived and designed the experiments; Analyzed and interpreted the data; Wrote the paper.

K. Bansura Banu: Performed the experiments; Wrote the paper.

Funding statement

This research did not receive any specific grant from funding agencies in the public, commercial, or not-for-profit sectors.

Competing interest statement

The authors declare no conflict of interest.

Additional information

No additional information is available for this paper.

References

[1] A. Hagfeldt, G. Boschloo, L. Sun, L. Kloo, H. Pettersson, Dye-sensitized solar cells, Chem. Rev. 110 (2010) 6595–6663.

[2] P. Surawatanawong, A.K. Wjcik, S. Kiatisevi, Density functional study of monobranched and di-branched di-anchoring triphenylamine cyanoacrylic dyes for dye-sensitized solar cells, J. Photochem. Photobiol., A 253 (2013) 62–71.

[3] S. Shi, Q. Liao, Y. Tang, H. Guo, X. Zhou, Y. Wang, T. Yang, Y. Liang, X. Cheng, F. Liu, X. Guo, Head-to-head linkage containing bithiophene-based polymeric semiconductors for highly efficient polymer solar cells, Adv. Mater. 28 (45) (2016) 9969–9977.

[4] J. Goldberger, D.J. Sirbuly, M. Law, P. Yang, ZnO nano wire transistors, J. Phys. Chem. B 109 (2005) 9.

[5] S. Aslanzadeh, Transition metal doped ZnO nanoclusters for carbon monoxide detection: DFT studies, J. Mol. Model. 22 (2016) 160.

[6] S. Sakthivel, B. Neppolian, M.V. Shankar, B. Arabindoo, M. Palanichamy, V. Murugesan, Solar photocatalytic degradation of azo dye: comparison of photo catalytic efficiency of ZnO and TiO_2, Sol. Energy Mater. Sol. Cells 77 (2003) 65–82.

[7] M.A. Abdulsattar, Chlorine gas reaction with ZnO wurtzoid nanocrystals as a function of temperature: a DFT study, J. Mol. Model. 23 (2017) 125.

[8] A.B. Patil, K.R. Patil, S.K. Pardeshi, Eco friendly synthesis and solar photo catalytic activity of S-doped ZnO, J. Hazard Mater. 183 (2010) 315.

[9] Anindita samanta, M.N. Goswami, P.K. Mahapatra, Magnetic and electric properties of Ni-doped ZnO nanoparticles exhibit diluted magnetic semiconductor in nature, J. Alloy. Comp. 730 (2018) 399–407.

[10] S. Fabbiyola, V. Sailaja, L. JohnKennedy, M. Bououdina, J. Judith Vijaya, Optical and magnetic properties of Ni-doped ZnO nanoparticles, J. Alloy. Comp. 694 (2017) 522–531.

[11] S. Pirillo, I. Lopez-Corral, E. German, A. Juan, Density functional study of Acrolein adsorption on Pt (111), Vacuum 99 (2014) 259–264.

[12] R. Ferullo, M.M. Branda, F. Illas, Coverage dependence of the structure of acrolein adsorbed on Ag (111), J. Phys. Chem. Lett. 1 (2010) 2546.

[13] Mehdi Yoosefian, Atef Pakpour, Nazanin Etminan, Nanofilter platform based on functionalized carbon nanotubes foe adsorption and elimination of Acrolein, a toxicant in cigarette smoke, Appl. Surf. Sci. 444 (2018) 598–603.

[14] M.J. Frisch, G.W. Trucks, H.B. Schlegel, G.E. Scuseria, M.A. Robb, J.R. Cheeseman, G. Scalmani, V. Barone, B. Mennucci, G.A. Peterson, H. Nakatsuji, M. Caricato, X. Li, H.P. Hratchian, A.F. Izmaylov, J. Bloino, G. Zheng, J.L. Sonnenberg, M. Hada, M. Ehara, K. Toyota, R. Fukuda, J. Hasegawa, M. Ishida, T. Nakajima, Y. Honda, O. Kitao, H. Nakai, T. Vreven, J.A. Montgomery Jr., J.E. Peralta, F. Ogliaro, M. Bearpark, J.J. Heyd, E. Brothers, K.N. Kudin, V.N. Staroverov, R. Kobayashi, J. Normand, K. Raghavachari, A. Rendell, J.C. Burant, S.S. Iyengar, J. Tomasi, M. Cossi, N. Rega, M.J. Millam, M. Klene, J.E. Knox, J.B. Cross, V. Bakken, C. Adamo, J. Jaramillo, R. Gomperts, R.E. Stratmann, O. Yazyev, A.J. Austin, R. Cammi, C. Pomeli, J.W. Ochterski, R.L. Martin, K. Morokuma, C.G. Zakrzewski, G.A. Voth, P. Salvador, J.J. Dannenberg, S. Dapprich, A.D. Daniels, O. Farkas, J.B. Foresman, J.V. Ortiz, J. Cioslowski, D.J. Fox, Gaussian 09, Revision D.01, Gaussian, Inc., Wallingford CT, 2009.

[15] N.M. O'Boyle, A.L. Tenderholt, K.M. Langner, Cclib: a library for package independent computational chemistry algorithm, J. Comput. Chem. 9 (2008) 839–845.

[16] Ali Shokuhi Rad, Khurshid Ayub, Ni adsorption on $Al_{12}P_{12}$ nano cage: DFT study, J. Alloy. Comp. 678 (2016) 317–324.

[17] Z.L. Wang, Zinc oxide nano structures: growth, properties and applications, J. Phys. Condens. Matter 16 (2004) 829–858.

[18] J. Beheshtian, A. Ahmadi Peyghan, Z. Bagheri, Adsorption and dissociation of Cl_2 molecule on ZnO nanocluster, Appl. Surf. Sci. 258 (2012) 8171–8176.

[19] Fatemeh Fallahpour, Milad Nouraliei, sara Soleimani Gorgani, Theoretical evaluation of a double functional heterogeneous nano sensors, Appl. Surf. Sci. 366 (2016) 545–551.

[20] S. Pal, A. Sarkar, Shallow acceptor state in ZnO realized by ion irradiation and annealing route, J. Alloy. Comp. 703 (2017) 26–33.

[21] T. Abram, S. Chitra, L. Bejjit, M. Bouachrine, T. Lakhlifi, Electronic and photovoltaic properties of new materials based on 6-mono substituted and 3,6-disubstituted acridines and their application to design novel materials, for organic solar cells, J. Comput. Methods Mol. Des. 4 (2014) 19–27.

[22] A. Mishra, P. Bauerla, Small molecule organic semiconductors on the move: promises for future solar energy technology, Angew. Chem. Int. Ed. 51 (2012) 2020–2067.

[23] C. Qin, A.E. Clark, DFT characterization of the optical and redox properties of natural pigments relevant to dye-sensitized solar cells, Chem. Phys. Lett. 438 (2007) 26.

[24] Hao Cui, Dachang Chen, Ying Zhang, Xiaoxing Zhang, Dissolved gas analysis in transformer oil using Pd catalyst decorated $MoSe_2$ monolayer: a first-principles theory, sus, Matr. Tech. 20 (2019), e00094.

[25] Hao Cui, Guozhi Zhang, Xiaoxing Zhang, Ju Tang, Rh-doped MoSe2 as a toxic gas scavenger: a first-principles study, Nanoscale Adv. 1 (2019) 772–780.

[26] Phool Singh Yadav, Dheeraj Kumar Pandey, A DFT study for the structural and electronic properties of Zn_mSe_n nanoclusters, Appl. Nanosci. 2 (2012) 351–357.

[27] Arab Ali, Mohaddeseh Habibzadeh, Theoretical study of geometry, stability and properties of Al and AlSi nanoclusters, J. Nanostruct. Chem. 6 (2016) 111–119.

[28] Robert G. Parr, Laszlo v. Szentpaly, Shubin Liu, Electrophilicity index, J. Am. Chem. Soc. 121 (1999) 1922–1924.

[29] R. Parthasarathi, J. padmanabhan, V. Subramaniam, U. Sarkar, B. Maiti, P.K. Chattaraj, Internet electron, J. Mol. Des. 2 (2003) 798–813.

[30] P.W. Ayers, J.S.M. Anderson, L.J. Bartolotti, Perturbative perspectives on the chemical reaction prediction problem, Int. J. Quantum Chem. 101 (2005) 520.

[31] G. Roos, S. Loverix, E. Brosens, K. Van Belle, L. Wyns, P. Geerlings, J. Messens, The activation of electrophile, nucleophile and leaving group during the reaction catalysed by pI258 arsenate reductase, Chem. Bio. Chem. 7 (2006) 981.

[32] V.L. Chandraboss, B. Karthikeyan, S. Senthilvelan, Experimental and first principle study of guanine adsorption on ZnO clusters, Phys. Chem. Chem. Phys. 16 (2014) 23461.

[33] Ali Shokuhi Rad, Khurshid Ayub, Detailed surface study of adsorbed nickel on $Al_{12}N_{12}$ nano cage, Thin Solid Films 612 (2016) 179–185.

[34] S. Dheivamalar, L. Sugi, K. Ambigai, Density functional theory study of exohedral carbon atoms effect on electrophilicity of nicotine: comparative analysis, Comput. Chem. 4 (2016) 17–31.

[35] Y. Hamada, Y. Nishimura, M. Tsuboi, In-plane vibrational modes of cytosine from an ab initio MO calculation, Chem. Phys. 100 (1985) 365–375.

[36] G.A. Osborne, Detection of triplet-singlet transitions by magnetic circular dichroism, with application to the spectrum of acrolein, J. Mol. Spectrosc. 49 (1974) 48–51.